

Article

Predicting the Printability of Poly(Lactide) Acid Filaments in Fused Deposition Modeling (FDM) Technology: Rheological Measurements and Experimental Evidence

Antonella Patti ^{1,*} , Stefano Acierno ² , Gianluca Cicala ¹  and Domenico Acierno ^{3,*} 

¹ Department of Civil Engineering and Architecture (DICAr), University of Catania, Viale Andrea Doria 6, 95125 Catania, Italy

² Department of Engineering, University of Sannio, Piazza Roma 21, 82100 Benevento, Italy

³ Regional Center of Competence New Technologies for Productive Activities Scarl, Via Nuova Agnano 11, 80125 Naples, Italy

* Correspondence: antonella.patti@unict.it (A.P.); acierno@crdctecnologie.it (D.A.)

Abstract: In this work, the authors aimed to identify a potential correlation between the printability and crucial rheological characteristics of materials involved in fused deposition modeling (FDM) technology. In this regard, three different poly(lactide) acid (PLA)-based filaments (two commercially available (here called V-PLA and R-PLA) and one processed in a lab-scale extruder (here called L-PLA)) have been considered. Dynamic rheological testing, in terms of frequency sweep at five different temperatures (130, 150, 170, 190, and 210 °C), was performed. Rheological properties expressed in terms of viscoelastic moduli and complex viscosity curves vs. frequency, characteristic relaxation times, activation energy (E_a), zero shear viscosity (η_0) and shear thinning index (n) were derived for each material. A characteristic relaxation time of around 0.243 s was found for V-PLA, a similar value (0.295 s) was calculated for R-PLA filaments, and a lower value of about an order of magnitude was calculated for L-PLA filament (~ 0.0303 s). The activation energy and shear thinning index resulted to be very comparable for all the filaments. On the contrary, V-PLA and R-PLA possessed a zero-shear viscosity ($\sim 10^4$ Pa*s at 170 °C) much higher than L-PLA ($\sim 10^3$ Pa*s). All the filaments were processed in a 3D printer, by attesting the effect of nozzle temperature (180, 190, and 210 °C, respectively) on printing process, and macroscopic shaping defects in printed objects. Final considerations allowed us to conclude that polymer relaxation time, zero-shear viscosity, and melt viscosity (affected by printing temperature) were critical parameters affecting the printing quality.

Keywords: 3D printing; poly(lactide) acid; rheological measurement; processing temperature; warpage



Citation: Patti, A.; Acierno, S.; Cicala, G.; Acierno, D. Predicting the Printability of Poly(Lactide) Acid Filaments in Fused Deposition Modeling (FDM) Technology: Rheological Measurements and Experimental Evidence. *ChemEngineering* **2023**, *7*, 1. <https://doi.org/10.3390/chemengineering7010001>

Received: 9 November 2022

Revised: 12 December 2022

Accepted: 19 December 2022

Published: 23 December 2022



Copyright: © 2022 by the authors. Licensee MDPI, Basel, Switzerland. This article is an open access article distributed under the terms and conditions of the Creative Commons Attribution (CC BY) license (<https://creativecommons.org/licenses/by/4.0/>).

1. Introduction

Firstly, developed by Stratasys, the fused deposition modeling (FDM) process allows for the fabrication of complex geometrical parts. This technology uses a wide range of materials, such as thermoplastics [1], composites [2], ceramics [3], metal particles [4], and also recycled [5] and filled polymers [6], to promote sustainable development. A wide range of applications are covered by FDM technology, such as in the aerospace [7], automotive [8], biomedical [9], and textile [10] industries.

The FDM method consists of the melting of a solid filament and forming it to produce a new shape. The filament is pushed through a drive wheel into a heated nozzle head, where it is transformed in liquid phase. Then, it comes out of the nozzle and is directed according to a specific geometry through a CAD drawing, to form ultra-thin layers, deposited one after the other [11].

Materials constituting the filament, structural parameters (i.e., raster angle, infill density, printing orientation, and stacking sequence), and manufacturing variables (i.e.,

printing speed, extrusion temperature and rate, layer thickness, nozzle transverse speed, and bed temperature) can play an important role in affecting the mechanical properties of FDM printed parts [12].

However, acting on printing parameters did not always allow us to eliminate defects that negatively affect the strength and appearance of the printed parts. These defects are represented by shape distortion (shrinkage, wrinkles, warping), internal micro/macro voids, poor bonding between layers, and surface roughness [13].

Perez et al. [14] demonstrated that the most important factors for controlling surface roughness are layer height and wall thickness in samples made from polylactic acid (PLA). On the contrary, no clear influence on surface roughness was verified by changing design pattern, printing speed, and temperature. Larger nozzle size and thicker layer height were found to decrease the micro voids space and quantity per unit area in the potential crack path by leading to a higher fatigue resistance in acrylonitrile butadiene styrene (ABS) printed specimens [15]. Simultaneous higher values of layer height and raster width increased the void formation by leading to a lower tensile strength in PLA-based 3D-printed components [16]. Distortion in 3D printed parts, made from PLA polymer, produced through the FDM method, as a function of layer thickness, nozzle temperature and scan, was investigated in [17]. The authors concluded that the lower the layer thickness, the higher the distortion of 3D objects due to an increased shrinkage effect. Then, the lower the nozzle temperature, in terms of difference in temperature between the nozzle and the surroundings, the lower the distortion. Distortion of printed pieces through the digital light processing (DLS) was mostly ascribed to material and stiffness of the structure [18]. Based on engineering experiences, this conclusion was extended to the most techniques belonging to the additive manufacturing (so also to the FDM). A detailed analysis, based on quantitative and qualitative models, to decrease the distortion in most additive manufacturing techniques, has been discussed in [19]. Here, the distortion of 3D objects was mainly attributed to the shrinkage tendency of each constituting layer of the 3D structure. The shrinkage of n layers was attributed to the stiffness of structures (deposited layers and support bed) and to the constraining force (magnitude and direction). This latter parameter was found to be dependent on constrain coefficient (influenced by heat source, the cooling conditions, the thermal physical properties of the material), coefficient of thermal expansion, temperature differences, shrinkage caused by phase transformation, modulus of deposited material, and cross-sectional area of the n layers. Finally, the part was deformed due to the inconsistent shrinkage, which was built from all layers' temporary shrinkage.

Successful bonding between two adjacent layers involves three phases: (1) surface contact, (2) neck growth driven by surface tension, and (3) molecular diffusion and entanglement across the inter-filament interface [20]. High print temperatures significantly speed up the diffusion [21], but can lead to polymer thermal aging and thermo-oxidative degradation [22], and can determine too-low viscosity of polymer melt that could be responsible of bubble formation and flow instability. Finally, high print temperatures also affect the dimensional accuracy of 3D printed parts. By increasing the polymer fluidity, higher deviation from the standard nominal size is proved [22]. Defects such as shrinkage and warpage have been considered to be caused by thermally induced stresses and strongly impact both dimensional accuracy and stability [23]. On the contrary, low processing temperatures can determine incomplete polymer melting and, consequently, points of failure, especially in the direction perpendicular to printing [24]. By decreasing the extruder temperatures, the production of organic volatile release in the atmosphere was also decreased [25]. Finally, too-low print temperatures can determine defects such as delamination and large gaps between raster lines [22]. The correct choice of the nozzle temperature and printing speed was found to significantly reduce the warping defects in 3D FDM parts [26].

According to the work by Jain et al. [27], the assessment of filament printability is based on different aspects. First, the melted material should be extruded from the nozzle with a stable flow. Then, once deposited on the heated platform, it should be able to

maintain the shape and to resist under the weight of multilayers deposited on it without deforming.

The viscoelastic properties of the molten polymer could be considered a useful help to control all these aspects. Specific viscosity values should be required to extrude melted polymer through the print nozzle (shear rate in the range of 30–500 s⁻¹ s) and during consolidation process upon deposition on the print bed (shear rate in the range of 0.01–0.1 s⁻¹) [28,29]. Appropriate material's characteristics, in terms of rheological features, have been considered essential to develop chosen geometry and performance in extrusion-based 3D printing process [29].

This study aims to investigate the printability of three different PLA-based filaments, two commercial materials and one produced in our laboratory. Polylactide acid is an aliphatic polyester, 100% coming from renewable sources such as corn starch and sugarcane. This polymer is a common thermoplastic often used in FDM process given the biodegradable features together with excellent mechanical properties [30]. Then, even if semicrystalline, PLA polymer possesses a low crystallization rate [31]. This is an important aspect to favor interlayer adhesion in 3D printed parts [32]. The designing of the printing temperature has been proposed through a better understanding of the processing-property relationships. In this regard, the rheological characteristics of three materials have been investigated over a range of temperature from 130 to 210 °C, and by applying the time-temperature superposition (TTS). This method was used to extend the frequency scale from 0.01 to 1000 rad/s, i.e., beyond that achievable with the experimental instrumentation (0.1–100 rad/s), so as to accomplish the typical shear rate encountered by the melted polymer during the printing process. Then, by fixing all the other printing parameters, various temperature conditions were chosen to extrude each material. The impact of processing temperatures on the printability of chosen filaments was based on the final appearance of 3D objects, and eventual defects perceptible to the naked eye. Experimental evidence related to printing defects were finally correlated to rheological properties

2. Materials and Methods

2.1. Materials

Three PLA-based filaments have been considered in this investigation: two commercially available filaments, supplied by EUMAKERS (Barletta, Italy), and one lab-made filament obtained by extruding a commercial-grade resin (cod. Ingeo™ Biopolymer 4032D, specific gravity 1.24 g/cm³) provided by Natureworks (Minnetonka, MN, USA). An extruder endowed with two intermeshing, co-rotating screws (mod. KETSE 20/40 D by Brabender, Duisburg, Germany) was used to process the PLA pellets. A filament, with a nominal appropriate size, for the available 3D printer (diameter of 1.75 mm), was realized. The extruder was operated with a motor speed equal to 30 rpm. Temperatures in the range from 180 to 210 °C were established for feed zone, the adapter and the die, and the melting zone, respectively. The melted material, coming out from extruder, was elongated and chilled in air by passing through the roller system. The first and second stretching speed of the motor drive were fixed at 1.5 and 2.5 rpm, respectively.

According to the manufacturer datasheet, the first commercial filament is made from PLA pellets (cod. Ingeo™ 4043D, density of 1.24 g/cm³ ASTM D792, MFR of 6 g/10 min ASTM D1238), produced by NatureWorks LLC, while the second one is realized by recovering the waste products from the filament manufacturing itself.

Preliminary characterization [33] allowed us to attest thermal properties (melting point, glass transition, an onset of thermal degradation) for three materials, summarized in Table 1.

Table 1. Thermal properties of three filaments: melting temperature (T_m), glass transition temperature (T_g), and initial decomposition temperature ($T_{dec5\%}$) in correspondence of 5% in mass loss.

Material	Name Abbreviation	T_g (°C)	T_m (°C)	$T_{dec5\%}$ (°C)
Virgin PLA filament	V-PLA	~60	150	313
Recycled PLA filament	R-PLA	~60	150	320
Lab-made PLA filament	L-PLA	65	170	267

2.2. Printing Process

The filaments were managed in printer (mod. M200) manufactured from Zortax (Olsztyn, Poland) through fused deposition modeling (FDM) technology. The set of the used printing parameters is summarized in Table 2. Prior to being further processed, the filaments were dried in an oven at temperature of 80 °C under vacuum for 10 h to remove moisture. Attempts to print 3D objects (Lego-type bricks) have been made at 180, 190 and 210 °C.

Table 2. Processing conditions to 3D printer.

Printing Parameters	
Layer thickness	0.09 mm
Infill density	100%
Design Pattern	Linear
Bed temperature	70 °C
First layer gap	0.30 mm
Printing speed	100 mm/s
Retraction distance	2.7 mm

2.3. Rotational Rheology

The linear viscoelastic properties of the (melted) filaments were measured by using a rotational rheometer (model ARES), produced by TA Instruments (New Castle, DE, USA). A geometry of parallel plate with nominal diameter of 25 mm was adopted. The heated chamber by forced convection was operated with gaseous nitrogen in order to prevent oxidation of the materials during the tests. Prior to the rheological experiments, all the materials were dried in a vacuum oven at 80 °C for 10 h. Furthermore, the thermal stability of the three materials was verified at temperatures up to 210 °C [33], and the linear viscoelastic regime was identified by strain amplitude sweep tests. The viscoelastic characterization was conducted by performing a series of tests (dynamic frequency sweep) in the frequency range from 0.1 to 100 rad/s at the temperatures of 130, 150, 170, 190, and 210 °C.

The time-temperature superposition (TTS) principle—which states an equivalence between changes in deformation rate and in temperature—was used to determine the rheological behaviour of the materials in a wider frequency (or time) domain.

3. Results

3.1. Experimental Evidence from 3D Printing Process: Warping Defects

Attempts to print the three considered filaments in a 3D object (Lego-type bricks) were conducted at distinct nozzle temperatures (180, 190, and 210 °C) and by maintaining the other process parameters fixed at the values indicated in Table 2. Images of final objects are reported in Figure 1.

In all cases, at a temperature of 180 °C, the printing process was never feasible. At this temperature, the material emerged from the duct with irregularities, settling in segments on the heated support and forming a non-continuous layer (as can be observed from Figure 1a).

By increasing the nozzle temperature at 190 °C, it was possible to extrude all the filaments, but a satisfactory finished 3D piece was achieved only in the case of lab-made

filament (L-PLA) while a significant warping (i.e., curling of the edges) can be noted for the bricks realized with V-PLA and R-PLA filaments. Furthermore, the brick made of R-PLA (Figure 1d) shows a higher degree of deformation compared to the one made from virgin PLA (Figure 1b).

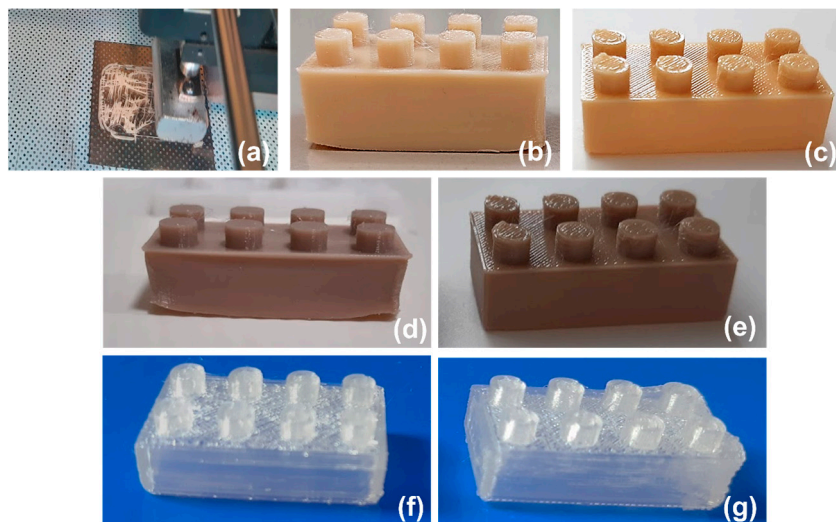


Figure 1. Attempts to print: V-PLA filament at 180 °C (a), 190 °C (b), and 210 °C (c); R-PLA at 190 °C (d) and 210 °C (e); L-PLA at 190 °C (f) and 210 °C (g).

The warping is a common defect in 3D objects, attributed to the internal thermal stress due to rapid heating and cooling, deformation and curling of corners [34]. In fact, once the filament is deposited on the heated platform (kept at a temperature lower than nozzle temperature), the molten polymer layer solidifies to form 3D printed object. During the cooling phase, phenomena such as volume contraction and shrinkage, could cause deformation in the final object, and thus warpage. The “volume contraction” is intended as a reduction in body volume, while “shrinkage” is associated to re-orientation, and relaxation of polymer chains (at constant volume) [35]. If the cooling does not occur uniformly across the 3D piece, differential shrinkage takes place, thus leading to wrapping [36]. Furthermore, residual thermal stresses can arise in the printed parts due to the temperature changes during the printing process, when the new melted filaments are deposited on previously deposited filaments, and restrict the corresponding volumetric changes [34]. The temperature increase in the printing chamber is often considered a practical solution to diminish the warping. It was observed that keeping the chamber at a higher temperature allows for a slower cooling of deposited layers and, consequently, determines fewer residual stresses and a lower shrinkage [37]. Warping in 3D printed parts depends on many process parameters, but it has been observed that a correct choice of nozzle temperature and printing speed reduces the warping defects significantly [26].

In our case, at a temperature of 210 °C, no curling of edges can be detected for V-PLA and R-PLA filaments (see Figure 1c,e, respectively), whereas a reduced dimensional accuracy due to a significant material’s deburring on the edges can be noted for L-PLA filament (see Figure 1g).

According to the literature of interest [38,39], warping deformation is evaluated as difference between two lengths, H and H_{\max} (Figure 2). Warping deformation are calculated for each edge of the 3D printed object and normalized with respect to the maximum height. Data are summarized in Table 3.

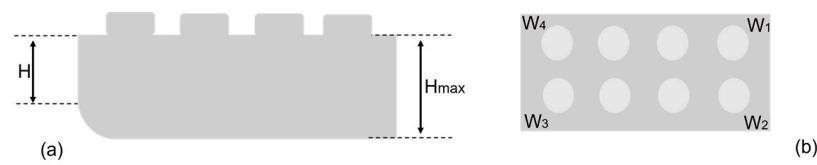


Figure 2. (a) Schematic of warping deformation ($W = H_{\max} - H$); (b) edges depiction of the 3D object used for measuring warpage.

Table 3. Warping deformation (%) ($W = \frac{H_{\max} - H}{H_{\max}} * 100$) for each edge (W_1, W_2, W_3, W_4) of 3D printed object at printing temperatures of 190 and 210 °C, respectively. Measurements have been conducted through the auxilium of a caliber.

	V-PLA		R-PLA		L-PLA	
	190 °C	210 °C	190 °C	210 °C	190 °C	210 °C
W_1	0%	0%	0%	0%	0%	0%
W_2	4.8%	0.9%	8.5%	0.2%	2.4%	1.1%
W_3	5.1%	1.1%	10.1%	0.6%	3.2%	2.9%
W_4	4.6%	0%	8.0%	0%	0.8%	0.8%

Measurements of the curling of corners for each edge of the 3D printed object at two printing temperatures (190 and 210 °C) confirmed evidence perceptible to the naked eye. Specifically, at a temperature of 210 °C, the warping effect was never detectable in each of the printed specimens, and lower height changes were recorded in R-PLA. On the contrary, at a lower printing temperature (190 °C), the strongest deformation was verified in correspondence of R-PLA ($W_2 = 10\%$).

3.2. Dynamic Rheological Measurements

The viscoelastic properties of all materials were assessed in the temperature range 130–210 °C. This constricted temperature range is mainly owing to the thermal instability of materials above 210 °C. The linear viscoelastic data show a thermorheologically simple behaviour that allows for the construction of master curves at a single reference temperature [40]. The master curves for the viscoelastic moduli and the complex viscosity are shown, at the reference temperature of 170 °C, in Figures 3 and 4, respectively.

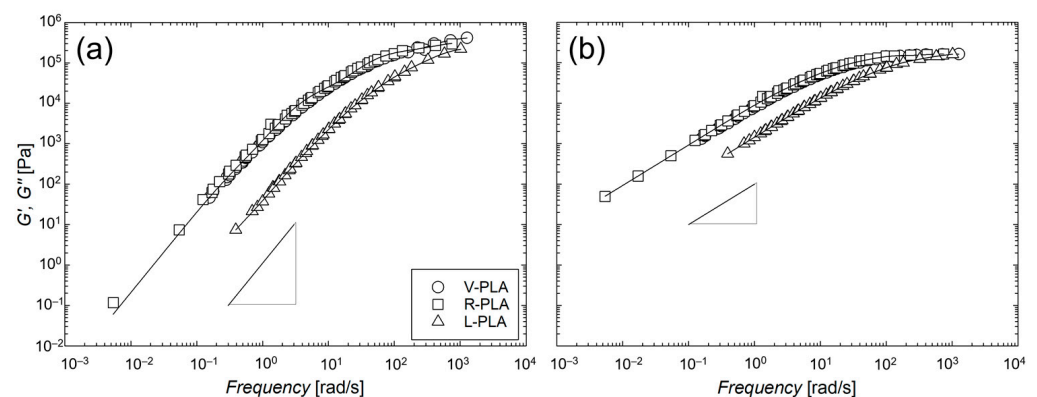


Figure 3. Master curve of storage G' (a) and loss G'' (b) moduli against reduced frequency of three materials at the reference temperature of 170 °C. The solid lines through data points represent best fitting with a 5-mode Maxwell model. Limiting slopes of 2 and 1 are also represented for comparison.

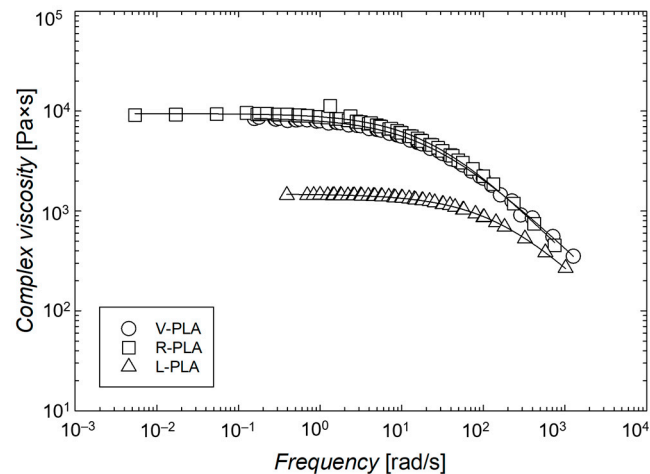


Figure 4. Reduced complex viscosity vs. reduced frequencies at the reference temperature $T_0 = 170\text{ }^\circ\text{C}$.

Figure 3 displayed the master curves of the storage (Figure 3a) and loss (Figure 3b) moduli at the reference temperature of $170\text{ }^\circ\text{C}$, as calculated from a generalized Maxwell spectrum. The linear viscoelastic behaviour of the three PLAs is typical of modestly entangled, linear polymer melts, with terminal regions (where G' is proportional to ω^2 and G'' to ω) clearly visible for both elastic and loss moduli in the low-frequency region. It should be observed that V- and R-PLA's have very similar moduli, while the L-PLA has lower moduli over the entire frequency range. This was attributed to greater molecular weight in V-PLA and R-PLA polymers compared to those possibly present in the L-PLA macromolecules. Furthermore, it can be observed that over the entire frequency range the materials show $G'' > G'$, thus suggesting a liquid-like behaviour and, according to Calafel et al. [41], feasibility of printing processes.

The experimentally determined dynamic moduli allow for the determination of a discrete relaxation spectrum; a nonlinear regression (using the method in [42]) allows for the calculation of a set of parameters to obtain a best fit of G' , G'' . Discrete relaxation spectra allow for the calculation of the zero-shear viscosity and the steady-state shear compliance according to the following formulas:

$$\eta_0 = \sum_{i=1}^N g_i \lambda_i \quad (1)$$

$$J_e^0 = \frac{\sum_{i=1}^N g_i \lambda_i^2}{\left(\sum_{i=1}^N g_i \lambda_i\right)^2} \quad (2)$$

where g_i and λ_i are the weighting modulus and the relaxation time corresponding to each Maxwell element. The characteristic relaxation time, defined as:

$$\lambda_c = \eta_0 J_e^0 \quad (3)$$

is considered as a reasonable approximation for the polymer's terminal relaxation time. Zero-shear viscosity, steady-state shear compliancy, and characteristic relaxation time are reported in Table 4 for all investigated materials.

The master curves for the reduced complex viscosity (η^*/a_T) as a function of reduced frequency ($a_T \cdot \omega^*$) at a reference temperature (T_0) of $170\text{ }^\circ\text{C}$ for all materials are reported in Figure 4.

All the materials show a Newtonian plateau at low deformation rates and a shear thinning behaviour at higher frequencies. In particular, V-PLA and R-PLA show very similar viscosities for the entire frequency range with a Newtonian (or zero-shear) viscosity

of about 10^4 Pa·s; L-PLA shows a lower Newtonian viscosity (about 1.5×10^3 Pa·s) and a transition toward the shear thinning zone shifted to higher frequencies with respect to V- and R-PLA. The reduced complex viscosity can be described using a Cross equation (Equation (4)).

$$\eta = \eta_{\infty} + \frac{\eta_0 - \eta_{\infty}}{1 + (\lambda\omega)^{1-n}} \quad (4)$$

where η_0 is the Newtonian (or zero-shear) viscosity, η_{∞} is the infinity viscosity assumed to be equal to zero (as usually conducted for polymer melts), and λ is a relaxation time that marks the transition to the shear-thinning regime.

Table 4. Viscoelastic parameters of the PLA's filaments, as referred at temperature of 170 °C.

	V-PLA	R-PLA	L-PLA
η_0 [Pa·s]	8500	9710	1470
λ_c [s]	0.243	0.295	0.0303
J_e^0 [10^5 /Pa]	2.86	3.04	2.07

Rheological parameters, in terms of η_0 , η_{∞} , ω_0 , n , calculated through the Cross model fitting of reduced viscosity curves, are summarized for all materials in Table 5. Data confirm on the one hand that V-PLA and R-PLA have very similar viscous properties over the entire deformation rates while, on the other hand, that L-PLA has a different behaviour with a viscosity much lower at low deformation rates and similar at higher rates.

Table 5. Rheological parameters by Cross model fitting of viscosity curves.

	η_0 (Pa·s)	λ (s)	n
V-PLA	8620	0.0781	0.325
R-PLA	9460	0.0830	0.291
L-PLA	1480	0.0131	0.371

The shear thinning behaviour has been considered a useful property of involved materials in the FDM technology since it helps the material flow in the nozzle at higher shear rate during the printing, and the retaining of the shape once the melted filament is deposited on the platform [43]. In this case, the shear-thinning index (n) was roughly similar for three examined filaments, whereas the zero-shear viscosity was approximately an order of magnitude greater for V-PLA and R-PLA than for L-PLA. This has been interpreted as the three polymers behaving similarly at higher shear rates (i.e., during the extrusion phase) and differently at lower shear rates (i.e., once deposited on the heated plate).

Variations in zero-shear viscosity can be linked to variations in molecular weight since the zero-shear viscosity for linear flexible polymers grows with a 3.4 power of the molecular weight [42] (as displayed in the Equation (5)). The observed differences in the rheological response can be related in particular to different molecular weights. In the work by Najafi et al. [44], the zero-shear viscosity (η_0) has been used to evaluate the molecular weight (M_w) of PLA polymer melts by using (Equation (5)):

$$\eta_0 = 10^{-14} M_w^{3.4} \quad (5)$$

The aforesaid correlation allowed us to evaluate a molecular weight equal to 1.88×10^5 g/mol for V-PLA, equal to 1.94×10^5 g/mol for R-PLA, and equal to 1.12×10^5 g/mol for L-PLA. These values confirm that the V- and the R-PLA have similar molecular weight while the L-PLA possesses a lower molecular weight.

In particular, viscoelastic data suggest that the molecular weights of virgin and recycled filament are very similar, with differences of the order of few percentages, while

the L-PLA has a molecular weight about 40% lower. Furthermore, differences in terms of characteristic relaxation are negligible when V- and R-PLA are compared but are remarkable when the L-PLA is compared to the others with the L-PLA having a much shorter relaxation time. In general, when the stress relaxation of the polymer chains is characterized by slow dynamics, frozen-in flow-induced stresses are generated and, consequently, an increase in warpage occurs [45]. In view of these considerations, it is possible to conclude that the higher degree of warping experimentally detected in 3D printing of R-PLA- and V-PLA-based objects at 190 °C compared to those made of L-PLA can be attributed to the lower ability of these polymers to relax the stresses. It could be considered that at a lower temperature (190 °C), a smaller zero-shear viscosity helped to relax thermal stress and reduce the warping phenomena. On the contrary, when the temperature was increased, the same parameter contributed to a slight loss of precision of fine details in shape (more rounded edges). In another words, a high value in zero-shear viscosity could help to maintain the shape of 3D objects, as the temperature was increased.

The activation energy represents the sensitivity of the material's viscoelastic properties to temperature changes (Figure 5). Small values of E_a , resulting in low sensitivity of viscosity to temperature, led to minimize stress concentration, crack formation, and distortion in the molded parts [46]. Materials with higher activation energy can show lower resistance to thermal stress and higher propensity to aesthetic defects (edge curling and warping). In the case of 3D printed parts, after layer deposition, a non-uniform cooling rate creates a temperature gradient by inducing residual thermal stress [47]. Furthermore, significant warpage was found in 3D printed parts made by materials with high crystallinity [48], and can be controlled by processing conditions such as layer thickness, bed temperature, heated chamber [49]. In our case, the activation energies of the three materials are very similar and the possible presence of warping in 3D final printed parts cannot be attributed to the different response of material's viscosity or to the temperature changes.

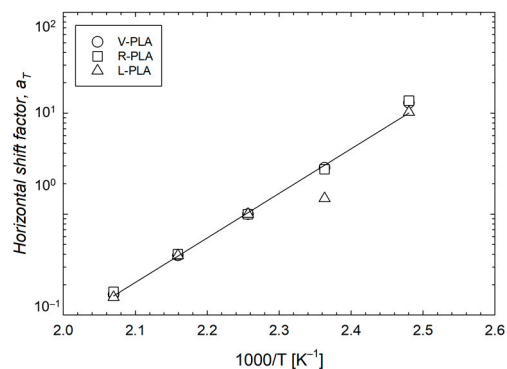


Figure 5. Horizontal shift factors vs. temperature.

The temperature dependency of viscoelastic properties is described by the horizontal shift factor (a_T) that, for the explored temperature range, shows an Arrhenius-like behaviour with an activation energy of 84 kJ/mol, evaluated through Equation (6):

$$a_T = \exp \left[\frac{E_a}{R} \left(\frac{1}{T} - \frac{1}{T_0} \right) \right] \quad (6)$$

in which E_a is the activation energy, R is the universal gas constant and T_0 is the reference temperature (here equal to 170 °C).

The assessed E_a value is in excellent agreement with values reported in literature for PLA (Al-Itry et al. [50] report 90 kJ/mol calculated on a close temperature interval). Furthermore, it should be mentioned that the three different PLAs show almost identical temperature dependency of the viscoelastic properties (i.e., same a_T 's and same vertical shift factors, b_T (the vertical shift factor is related to variations in the density and in our case, as expected, is very close to unity)).

According to rheometry (see for instance [51]), the apparent shear rate $\dot{\gamma}_{app}$ at the nozzle is estimated using Equation (7):

$$\dot{\gamma}_{app} = \frac{4Q}{\pi R^3} \quad (7)$$

where Q is the volumetric flow rate evaluated as nozzle cross-section ($A = \pi R^2$, R is the nozzle radius) multiplied for the printing speed v_{print} .

For the true shear rate, the following equation can be used for a power law fluid:

$$\dot{\gamma} = \dot{\gamma}_{app} \left(\frac{3n+1}{4n} \right) \quad (8)$$

In our case, the nozzle diameter being equal to 0.4 mm and the printing speed left to the default value (100 mm/s), the apparent shear rate at the nozzle is in the range of 2000 s^{-1} . By considering the evaluated power index for each polymer, no strong difference existed among the true shear rates (3000 s^{-1}) and viscosity data (order of magnitude = $10^2 \text{ Pa}\cdot\text{s}$) of three filaments.

On the other hand, the pressure drop (ΔP) encountered by a non-Newtonian fluid across the conduit (of radius R and length L) can roughly be estimated by the following equation (Equation (9)):

$$\Delta P = \frac{8Q\eta L}{\pi R^4} \left(\frac{3n+1}{4n} \right) \quad (9)$$

According to this consideration, by fixing the 3D printer apparatus (i.e., diameter and length, and maximum allowable pressure), to ensure a continuous material flow along the conduit, the following condition should be respected (Equation (10)):

$$\frac{2Q\eta L}{\pi R^4} \left(\frac{3n+1}{n} \right) \leq \Delta P^{\max} \quad (10)$$

and so (Equation (11)):

$$v_{print}\eta \leq \frac{\Delta P^{\max} R^2}{2L} \left(\frac{n}{3n+1} \right) \quad (11)$$

Finally, it can be concluded that, given the 3D printer set-up, the combination between the material viscosity and the selected printing speed was the main technological parameter to play an important role in guaranteeing a continuous flow of material during the printing. Usually, too-low printing speed was never chosen so to avoid too-high processing time.

The residence time (τ) of polymer within a barrel of 35 mm length and 1 mm radius (barrel volume: V_{barrel}) was estimated to be around 10 s (Equation (12)):

$$\tau = \frac{V_{barrel}}{Q} \quad (12)$$

Then, it can be taken as reference the following physical properties of PLA polymer: thermal conductivity of $0.13 \text{ W}/(\text{m K})$, specific heat of $1800 \text{ J}/(\text{Kg K})$ and density of $1220 \text{ kg}/\text{m}^3$ [52].

By unsteady thermal conduction in solid (cylindrical geometry), when the external surface was kept at constant temperature (extrusion temperature) of $180 \text{ }^\circ\text{C}$, the temperature achieved in the centre was around $170 \text{ }^\circ\text{C}$ (sufficiently around polymer melting point).

Based on these findings, the residence time and thus the printing speed (also in terms of volumetric flow rate) were deemed adequate to ensure that the polymer inside the barrel was fully melted. As a result, in order to guarantee polymer printability, it occurred to act on the viscoelastic properties of polymers via the printing temperature.

4. Conclusions

This work aimed to investigate the processability of three different poly(lactide) acid (PLA)-based filaments through fused deposition modeling (FDM). All systems were worked in a 3D printing machine by changing the nozzle temperature (180, 190, and 210 °C, respectively) and by observing aesthetic defects perceptible to the naked eye in printed parts.

Macroscopic defects (i.e., warping) were observed in 3D objects at a fixed extruder temperature (190 °C), when the material possessed characteristic relaxation times of polymer chains around 2×10^{-1} s, in combination with elevated η_0 values of 10^4 Pa*s (i.e., molecular weight (M_w) of 1.94×10^5 g/mol). Even in the case of almost the same values in E_a (~80–90 KJ/mol) (i.e., sensitivity of viscosity to temperature changes), if the polymer chains possessed a lower relaxation time (around 10^{-2} s) and η_0 values in the order of magnitude of 10^3 Pa*s (i.e., $M_w = 1.12 \times 10^5$ g/mol), the material's response to thermal stress was improved, and also at a lower nozzle temperature (190 °C) no signs of warpage were observed.

Then, it was found that, once the physical characteristics of the printer had been established (i.e., diameter and length of nozzle, and maximum allowable pressure drop), a specific combination of materials' viscosity ($\sim 10^2$ Pa*s) and printing speed (i.e., 100 mm/s) could lead to a discontinuous flow of molten polymer from the duct determining a failure in the printing process. Calculations on the heat conduction in the solid as well as material residence time of the polymer inside the barrel allowed us to rule out the possibility of not thoroughly melting the polymer inside the barrel.

Therefore, it was concluded that polymer relaxation time and zero-shear viscosity were considered two crucial aspects during the deposition of the material on the heated support to limit deformation and warping defect into 3D printed structures, and the main parameter to control the printability of filaments during the extrusion was material viscosity (affected by printing temperature).

Author Contributions: Conceptualization, A.P. and D.A.; validation, G.C.; data curation, S.A. and A.P. writing—original draft preparation, A.P.; writing—review and editing, S.A. and G.C.; supervision, D.A. All authors have read and agreed to the published version of the manuscript.

Funding: This research received no external funding.

Institutional Review Board Statement: Not applicable.

Informed Consent Statement: Not applicable.

Data Availability Statement: The data presented in this study are available on request from the corresponding author.

Acknowledgments: A. Patti wishes to thank the Italian Ministry of Education, Universities and Re-search (MIUR) in the framework of Action 1.2 “Researcher Mobility” of The Axis I of PON R&I 2014-142 2020 under the call “AIM—Attrazione e Mobilità Internazionale”. S. Acierno and G. Cicala acknowledge the support of the Italian Ministry of University, project PRIN 2017, 20179SWLKA “Multiple Advanced Materials Manufactured by Additive technologies (MAMMA)”.

Conflicts of Interest: The authors declare no conflict of interest.

References

1. Garzon-Hernandez, S.; Arias, A.; Garcia-Gonzalez, D. A continuum constitutive model for FDM 3D printed thermoplastics. *Compos. Part B Eng.* **2020**, *201*, 108373. [[CrossRef](#)]
2. Liu, Z.; Lei, Q.; Xing, S. Mechanical characteristics of wood, ceramic, metal and carbon fiber-based PLA composites fabricated by FDM. *J. Mater. Res. Technol.* **2019**, *8*, 3741–3751. [[CrossRef](#)]
3. Chen, Z.; Li, Z.; Li, J.; Liu, C.; Lao, C.; Fu, Y.; Liu, C.; Li, Y.; Wang, P.; He, Y. 3D printing of ceramics: A review. *J. Eur. Ceram. Soc.* **2019**, *39*, 661–687. [[CrossRef](#)]
4. Patti, A.; Cicala, G.; Tosto, C.; Saitta, L.; Acierno, D. Characterization of 3D Printed Highly Filled Composite: Structure, Thermal Diffusivity and Dynamic-Mechanical Analysis. *Chem. Eng. Trans.* **2021**, *86*, 1537–1542. [[CrossRef](#)]
5. Patti, A.; Acierno, S.; Cicala, G.; Acierno, D. Recycling waste from film packaging to 3D printing applications: A prospective study to identify the processing temperature. *Chem. Eng. Trans.* **2022**, *96*, 55–60.

6. Omar, N.W.Y.; Shuaib, N.A.; Hadi, M.H.J.A.; Azmi, A.I.; Misbah, M.N. Mechanical and Physical Properties of Recycled-Carbon-Fiber-Reinforced Polylactide Fused Deposition Modelling Filament. *Materials* **2021**, *15*, 190. [[CrossRef](#)]
7. Pascariu, I.S.; Zaharia, S.M. Design and Testing of an Unmanned Aerial Vehicle Manufactured by Fused Deposition Modeling. *J. Aerosp. Eng.* **2020**, *33*, 06020002. [[CrossRef](#)]
8. Yadav, D.K.; Srivastava, R.; Dev, S. Design & fabrication of ABS part by FDM for automobile application. *Mater. Today Proc.* **2020**, *26*, 2089–2093. [[CrossRef](#)]
9. Cali, M.; Pascoletti, G.; Gaeta, M.; Milazzo, G.; Ambu, R. New filaments with natural fillers for FDM 3D printing and their applications in biomedical field. *Procedia Manuf.* **2020**, *51*, 698–703. [[CrossRef](#)]
10. Patti, A.; Acierno, D. Towards the Sustainability of the Plastic Industry through Biopolymers: Properties and Potential Applications to the Textiles World. *Polymers* **2022**, *14*, 692. [[CrossRef](#)]
11. Kristiawan, R.B.; Imaduddin, F.; Ariawan, D.; Ubaidillah; Arifin, Z. A review on the fused deposition modeling (FDM) 3D printing: Filament processing, materials, and printing parameters. *Open Eng.* **2021**, *11*, 639–649. [[CrossRef](#)]
12. Cano-Vicent, A.; Tambuwala, M.M.; Hassan, S.S.; Barh, D.; Aljabali, A.A.A.; Birkett, M.; Arjunan, A.; Serrano-Aroca, Á. Fused deposition modelling: Current status, methodology, applications and future prospects. *Addit. Manuf.* **2021**, *47*, 102378. [[CrossRef](#)]
13. Wickramasinghe, S.; Do, T.; Tran, P. FDM-Based 3D Printing of Polymer and Associated Composite: A Review on Mechanical Properties, Defects and Treatments. *Polymers* **2020**, *12*, 1529. [[CrossRef](#)]
14. Pérez, M.; Medina-Sánchez, G.; García-Collado, A.; Gupta, M.; Carou, D. Surface Quality Enhancement of Fused Deposition Modeling (FDM) Printed Samples Based on the Selection of Critical Printing Parameters. *Materials* **2018**, *11*, 1382. [[CrossRef](#)] [[PubMed](#)]
15. He, F.; Khan, M.; Sapuan, M.; Ilyas, R.A. Effects of Printing Parameters on the Fatigue Behaviour of 3D-Printed ABS under Dynamic Thermo-Mechanical Loads. *Polymers* **2021**, *13*, 2362. [[CrossRef](#)] [[PubMed](#)]
16. Rajpurohit, S.R.; Dave, H.K. Analysis of tensile strength of a fused filament fabricated PLA part using an open-source 3D printer. *Int. J. Adv. Manuf. Technol.* **2018**, *101*, 1525–1536. [[CrossRef](#)]
17. Xinhua, L.; Li, S.; Zhou, L.; Xianhua, Z.; Xiaohu, C.; Zhongbin, W. An investigation on distortion of PLA thin-plate part in the FDM process. *Int. J. Adv. Manuf. Technol.* **2015**, *79*, 1117–1126. [[CrossRef](#)]
18. Wu, D.; Zhao, Z.; Zhang, Q.; Qi, H.J.; Fang, D. Mechanics of shape distortion of DLP 3D printed structures during UV post-curing. *Soft Matter* **2019**, *15*, 6151–6159. [[CrossRef](#)]
19. Xie, D.; Lv, F.; Liang, H.; Shen, L.; Tian, Z.; Zhao, J.; Song, Y.; Shuai, C. Towards a comprehensive understanding of distortion in additive manufacturing based on assumption of constraining force. *Virtual Phys. Prototyp.* **2021**, *16*, S85–S97. [[CrossRef](#)]
20. Gao, X.; Qi, S.; Kuang, X.; Su, Y.; Li, J.; Wang, D. Fused filament fabrication of polymer materials: A review of interlayer bond. *Addit. Manuf.* **2021**, *37*, 101658. [[CrossRef](#)]
21. McIlroy, C.; Olmsted, P.D. Disentanglement effects on welding behaviour of polymer melts during the fused-filament-fabrication method for additive manufacturing. *Polymer* **2017**, *123*, 376–391. [[CrossRef](#)]
22. Frunzaverde, D.; Cojocar, V.; Ciubotariu, C.-R.; Miclosina, C.-O.; Ardeljan, D.D.; Ignat, E.F.; Marginean, G. The Influence of the Printing Temperature and the Filament Color on the Dimensional Accuracy, Tensile Strength, and Friction Performance of FFF-Printed PLA Specimens. *Polymers* **2022**, *14*, 1978. [[CrossRef](#)] [[PubMed](#)]
23. Gou, G.; Xie, P.; Yang, W.; Ding, Y. Online measurement of rheological properties of polypropylene based on an injection molding machine to simulate the injection-molding process. *Polym. Test.* **2011**, *30*, 826–832. [[CrossRef](#)]
24. Schirmeister, C.G.; Hees, T.; Licht, E.H.; Mülhaupt, R. 3D printing of high density polyethylene by fused filament fabrication. *Addit. Manuf.* **2019**, *28*, 152–159. [[CrossRef](#)]
25. Patti, A.; Acierno, S.; Cicala, G.; Tuccitto, N.; Acierno, D. Refining the 3D Printer Set-up to Reduce the Environmental Impact of the Fused Deposition Modelling (fdm) Technology. *Chem. Eng. Trans.* **2022**, *91*, 415–420. [[CrossRef](#)]
26. Alsoufi, M.S.; El-Sayed, A. Warping Deformation of Desktop 3D Printed Parts Manufactured by Open Source Fused Deposition Modeling (FDM) System. *Int. J. Mech. Mechatron. Eng.* **2017**, *17*, 7–16.
27. Jain, T.; Tseng, Y.M.; Tantisuwanno, C.; Menefee, J.; Shahrokhian, A.; Isayeva, I.; Joy, A. Synthesis, Rheology, and Assessment of 3D Printability of Multifunctional Polyesters for Extrusion-Based Direct-Write 3D Printing. *ACS Appl. Polym. Mater.* **2021**, *3*, 6618–6631. [[CrossRef](#)]
28. Gilmer, E.L.; Mansfield, C.; Gardner, J.M.; Siochi, E.J.; Baird, D.G.; Bortner, M.J. Characterization and Analysis of Polyetherimide: Realizing Practical Challenges of Modeling the Extrusion-Based Additive Manufacturing Process. *ACS Symp. Ser.* **2019**, *1315*, 69–84. [[CrossRef](#)]
29. Das, A.; Gilmer, E.L.; Biria, S.; Bortner, M.J. Importance of Polymer Rheology on Material Extrusion Additive Manufacturing: Correlating Process Physics to Print Properties. *ACS Appl. Polym. Mater.* **2021**, *3*, 1218–1249. [[CrossRef](#)]
30. Musa, L.; Krishna Kumar, N.; Abd Rahim, S.Z.; Mohamad Rasidi, M.S.; Watson Rennie, A.E.; Rahman, R.; Yousefi Kanani, A.; Azmi, A.A. A review on the potential of polylactic acid based thermoplastic elastomer as filament material for fused deposition modelling. *J. Mater. Res. Technol.* **2022**, *20*, 2841–2858. [[CrossRef](#)]
31. Patti, A.; Acierno, S.; Cicala, G.; Zarrelli, M.; Acierno, D. Recovery of Waste Material from Biobags: 3D Printing Process and Thermo-Mechanical Characteristics in Comparison to Virgin and Composite Matrices. *Polymers* **2022**, *14*, 1943. [[CrossRef](#)]
32. Shang, Y.; Xu, Q.; Jiang, B.; Yang, Y.; Liu, X.; Jiang, Z.; Yu, C.; Li, X.; Zhang, H. Slowing crystallization to enhance interlayer strength of 3D printed poly (ether ether ketone) parts by molecular design. *Addit. Manuf.* **2022**, *59*, 103104. [[CrossRef](#)]

33. Patti, A.; Aciermo, S.; Cicala, G.; Zarrelli, M.; Aciermo, D. The Understanding the Processing Window of Virgin and Recycled Bio-based Filaments for 3D Printing Applications. *Macromol. Symp.* **2022**, *405*, 2100291. [[CrossRef](#)]
34. Quelho de Macedo, R.; Ferreira, R.T.L.; Jayachandran, K. Determination of mechanical properties of FFF 3D printed material by assessing void volume fraction, cooling rate and residual thermal stresses. *Rapid Prototyp. J.* **2019**, *25*, 1661–1683. [[CrossRef](#)]
35. Koslowski, T.; Bonten, C. Shrinkage, warpage and residual stresses of injection molded parts. *AIP Conf. Proc.* **2019**, *2055*, 070003. [[CrossRef](#)]
36. Samy, A.A.; Golbang, A.; Harkin-Jones, E.; Archer, E.; Tormey, D.; McIlhagger, A. Finite element analysis of residual stress and warpage in a 3D printed semi-crystalline polymer: Effect of ambient temperature and nozzle speed. *J. Manuf. Process.* **2021**, *70*, 389–399. [[CrossRef](#)]
37. Spoerk, M.; Gonzalez-Gutierrez, J.; Sapkota, J.; Schuschnigg, S.; Holzer, C. Effect of the printing bed temperature on the adhesion of parts produced by fused filament fabrication. *Plast. Rubber Compos.* **2017**, *47*, 17–24. [[CrossRef](#)]
38. Ramian, J.; Ramian, J.; Dziob, D. Thermal Deformations of Thermoplast during 3D Printing: Warping in the Case of ABS. *Materials* **2021**, *14*, 7070. [[CrossRef](#)]
39. Nazan, M.A.; Ramli, F.R.; Alkahari, M.R.; Sudin, M.N.; Abdullah, M.A. Process parameter optimization of 3D printer using response surface method. *J. Eng. Appl. Sci.* **2017**, *12*, 2291–2296.
40. Ferry, J.D. *Viscoelastic Properties of Polymers*, 3rd ed.; John Wiley & Sons: New York, NY, USA, 1980; ISBN 978-0-471-04894-7.
41. Calafel, I.; Aguirresarobe, R.H.; Peñas, M.I.; Santamaria, A.; Tierno, M.; Conde, J.I.; Pascual, B. Searching for Rheological Conditions for FFF 3D Printing with PVC Based Flexible Compounds. *Materials* **2020**, *13*, 178. [[CrossRef](#)]
42. Baumgaertel, M.; Winter, H.H. Determination of discrete relaxation and retardation time spectra from dynamic mechanical data. *Rheol. Acta* **1989**, *28*, 511–519. [[CrossRef](#)]
43. Nguyen, N.A.; Bowland, C.C.; Naskar, A.K. A general method to improve 3D-printability and inter-layer adhesion in lignin-based composites. *Appl. Mater. Today* **2018**, *12*, 138–152. [[CrossRef](#)]
44. Najafi, N.; Heuzey, M.C.; Carreau, P.J.; Wood-Adams, P.M. Control of thermal degradation of polylactide (PLA)-clay nanocomposites using chain extenders. *Polym. Degrad. Stab.* **2012**, *97*, 554–565. [[CrossRef](#)]
45. DePolo, W.S.; Baird, D.G. Flow-induced warpage of injection-molded TLCP fiber-reinforced polypropylene composites. *Polym. Compos.* **2006**, *27*, 239–248. [[CrossRef](#)]
46. Khakbiz, M.; Simchi, A.; Bagheri, R. Analysis of the rheological behavior and stability of 316L stainless steel-TiC powder injection molding feedstock. *Mater. Sci. Eng. A* **2005**, *407*, 105–113. [[CrossRef](#)]
47. Ghnatio, C.; Fayazbakhsh, K. Warping estimation of continuous fiber-reinforced composites made by robotic 3D printing. *Addit. Manuf.* **2022**, *55*, 102796. [[CrossRef](#)]
48. Candal, M.V.; Calafel, I.; Aranburu, N.; Fernández, M.; Gerrica-Echevarria, G.; Santamaria, A.; Müller, A.J. Thermo-rheological effects on successful 3D printing of biodegradable polyesters. *Addit. Manuf.* **2020**, *36*, 101408. [[CrossRef](#)]
49. Winter, K.; Wilfert, J.; Häupler, B.; Erlmann, J.; Altstädt, V. Large Scale 3D Printing: Influence of Fillers on Warp Deformation and on Mechanical Properties of Printed Polypropylene Components. *Macromol. Mater. Eng.* **2022**, *307*, 2100528. [[CrossRef](#)]
50. Al-Itry, R.; Lamnawar, K.; Maazouz, A. Reactive extrusion of PLA, PBAT with a multi-functional epoxide: Physico-chemical and rheological properties. *Eur. Polym. J.* **2014**, *58*, 90–102. [[CrossRef](#)]
51. Macosko, C.W. *Rheology: Principles, Measurements, and Applications*; John Wiley & Sons, Inc.: New York, NY, USA, 1994; ISBN 978-0-471-18575-8.
52. Haleem, A.; Kumar, V.; Kumar, L. Mathematical Modelling & Pressure Drop Analysis of Fused Deposition Modelling Feed Wire. *Int. J. Eng. Technol.* **2017**, *9*, 2885–2894. [[CrossRef](#)]

Disclaimer/Publisher’s Note: The statements, opinions and data contained in all publications are solely those of the individual author(s) and contributor(s) and not of MDPI and/or the editor(s). MDPI and/or the editor(s) disclaim responsibility for any injury to people or property resulting from any ideas, methods, instructions or products referred to in the content.